

An anti-aliasing filtering of quantum images in spatial domain using a pyramid structure

Kai Wu(吴凯), Rigui Zhou(周日贵), and Jia Luo(罗佳)

Citation: Chin. Phys. B, 2024, 33 (**5**): 050305. DOI: 10.1088/1674-1056/ad2504
Journal homepage: http://cpb.iphy.ac.cn; http://iopscience.iop.org/cpb

What follows is a list of articles you may be interested in

Non-Gaussian quantum states generated via quantum catalysis and their statistical properties

Xiao-Yan Zhang(张晓燕), Chun-Yan Yang(杨春燕), Ji-Suo Wang(王继锁), and Xiang-Guo Meng(孟祥国)
Chin. Phys. B, 2024, 33 (**4**): 040308. DOI: 10.1088/1674-1056/ad2a74

Preparing highly entangled states of nanodiamond rotation and NV center spin

Wen-Liang Li(李文亮) and Duan-Lu Zhou(周端陆)
Chin. Phys. B, 2024, 33 (**2**): 020305. DOI: 10.1088/1674-1056/ad117a

Holevo bound independent of weight matrices for estimating two parameters of a qubit

Chang Niu(牛畅) and Sixia Yu(郁司夏)
Chin. Phys. B, 2024, 33 (**2**): 020304. DOI: 10.1088/1674-1056/ad117d

Generalized uncertainty principle from long-range kernel effects: The case of the Hawking black hole temperature

Rami Ahmad El-Nabulsi and Waranont Anukool
Chin. Phys. B, 2023, 32 (**9**): 090303. DOI: 10.1088/1674-1056/acac15

Quantum legitimacy of reversible gate and a new design of multiplier based on R gate

Tingyu Ge(葛庭宇), Tinggui Zhang(张廷桂), Xiaofen Huang(黄晓芬)
Chin. Phys. B, 2020, 29 (**5**): 050305. DOI: 10.1088/1674-1056/ab7d9d

---

An anti-aliasing filtering of quantum images in spatial domain using a pyramid structure

Kai Wu(吴凯)[1,2], Rigui Zhou(周日贵)[1,2,†], and Jia Luo(罗佳)[2,3,‡]

[1] *College of Information Engineering, Shanghai Maritime University, Shanghai* 201306, *China*
[2] *Research Center of Intelligent Information Processing and Quantum Intelligent Computing, Shanghai* 201306, *China*
[3] *School of Mathematics and Computational Science, Shangrao Normal University, Shangrao* 334001, *China*

(Received 22 November 2023; revised manuscript received 23 January 2024; accepted manuscript online 2 February 2024)

As a part of quantum image processing, quantum image filtering is a crucial technology in the development of quantum computing. Low-pass filtering can effectively achieve anti-aliasing effects on images. Currently, most quantum image filterings are based on classical domains and grayscale images, and there are relatively fewer studies on anti-aliasing in the quantum domain. This paper proposes a scheme for anti-aliasing filtering based on quantum grayscale and color image scaling in the spatial domain. It achieves the effect of anti-aliasing filtering on quantum images during the scaling process. First, we use the novel enhanced quantum representation (NEQR) and the improved quantum representation of color images (INCQI) to represent classical images. Since aliasing phenomena are more pronounced when images are scaled down, this paper focuses only on the anti-aliasing effects in the case of reduction. Subsequently, we perform anti-aliasing filtering on the quantum representation of the original image and then use bilinear interpolation to scale down the image, achieving the anti-aliasing effect. The constructed pyramid model is then used to select an appropriate image for upscaling to the original image size. Finally, the complexity of the circuit is analyzed. Compared to the images experiencing aliasing effects solely due to scaling, applying anti-aliasing filtering to the images results in smoother and clearer outputs. Additionally, the anti-aliasing filtering allows for manual intervention to select the desired level of image smoothness.

Keywords: quantum color image processing, anti-aliasing filtering algorithm, quantum multiplier, pyramid model

PACS: 03.67.–a, 03.67.Ac, 03.67.Lx, 07.05.Pj **DOI:** 10.1088/1674-1056/ad2504

1. Introduction

Quantum computing, as an emerging field, has gained increasing attention due to its distinctiveness from classical computing, particularly its high level of parallelism. The interest in quantum computing escalated since 1982 when Feynman proposed a new computing model[1] and named it the quantum computer. In 1985, the concept of a quantum Turing machine was introduced for the first time.[2] With the advantages of quantum computing, numerous quantum algorithms have emerged, such as Shor's algorithm for large integer factorization,[3] Grover's algorithm for quadratic speedup in database searches,[4] and the quantum Fourier transform algorithm. These algorithms demonstrate the superior capabilities of quantum computers over classical computers.

Building upon the innovative strides in quantum computing, the challenges faced by neural network-based machine learning in the quantum physics realm have led to the development of groundbreaking solutions. A notable example is the quantum convolutional neural network (QCNN),[5] introduced in response to the exponential complexity of many-body systems. Inspired by advancements in quantum information processors, the QCNN employs a quantum circuit-based algorithm, leveraging insights from convolutional neural networks. This quantum-enhanced approach stands out for its efficiency, utilizing only $O(\log N)$ variational parameters for N qubits, thereby facilitating effective training on practical quantum devices. Capabilities of the QCNN extend to the precise recognition of quantum states associated with a one-dimensional symmetry-protected topological phase, surpassing conventional methods. Furthermore, the QCNN exhibits exceptional performance in the realm of quantum error correction, outclassing established codes. The research in neural networks remains a vibrant and dynamic field, characterized by a multitude of relevant studies.[6–10] These innovations represent significant advancements in leveraging quantum technologies for computation, machine learning, and image processing.

Next, we delve into the significant innovations and applications that quantum computing has achieved in the representation and processing of images. Various quantum image representation models have been proposed, including qubit lattice,[11] entangled images,[12] real ket,[13] flexible representation of quantum images,[14] new quantum-enhanced representation (NEQR),[15] quantum image representation of logarithmic polar images,[16] and an improved novel quantum color image representation model (INCQI).[17] Based on these representation

†Corresponding author. E-mail: rgzhou@shmtu.edu.cn
‡Corresponding author. E-mail: luojia2227@163.com

© 2024 Chinese Physical Society and IOP Publishing Ltd

models, numerous quantum image processing algorithms have emerged, covering areas such as quantum grayscale and color image scaling,[18–21] quantum image feature extraction,[22,23] quantum image transformation,[24–26] quantum image matching,[27–29] quantum image compression,[30] quantum image segmentation,[30,31] quantum image watermarking,[32–37] and quantum image encryption.[38–40]

In image processing, aliasing is a common phenomenon occurring when an image is sampled or scaled, resulting in high-frequency information being erroneously represented as low-frequency information, leading to unnatural artifacts or distortions. To mitigate or avoid aliasing, anti-aliasing techniques are employed. Anti-aliasing is an image processing method designed to preprocess images to prevent aliasing issues after sampling or scaling. This technique effectively improves image quality, preserving details and clarity without introducing additional distortions or artifacts, which is crucial for maintaining high-quality and accurate images, especially in tasks requiring image analysis and visual perception. Common anti-aliasing methods include filtering, a prevalent technique for altering the frequency characteristics of images, emphasizing or attenuating specific features. Image filters can be considered as special mathematical functions applied to each pixel or a group of pixels through convolution operations in image processing. Different types of filter kernel functions yield various filtering effects, making the selection of appropriate filters a crucial step in image processing. Common image filters include mean filters, Gaussian filters, Sobel filters, among others. In summary, image filtering is a fundamental technique in image processing, aiding in improving image quality, reducing noise, and highlighting features, providing a better foundation for subsequent image analysis and visual tasks.

However, research on quantum image anti-aliasing processing is relatively scarce today because achieving anti-aliasing low-pass filtering requires operations related to correlation or convolution, which have been proven to be impossible in quantum implementation due to linear restrictions.[41] In 2017, Yuan *et al.* proposed spatial domain quantum image filtering,[42] replacing quantum multiplication with quantum addition to perform element-wise multiplication between neighborhood images and filter masks. Nevertheless, this method has two drawbacks: (1) Specific filter coefficients must be known before the filtering operation. (2) This method is only applicable to integer filter coefficients, not decimal ones. Subsequently, Yuan *et al.* proposed an improved spatial domain quantum image filtering inspired by binary multiplication,[43] presenting a novel approach for spatial domain anti-aliasing filtering to address these issues by designing a quantum adder combined with a right shift operator for quantum multiplication.

This paper introduces a novel spatial-domain quantum grayscale and color image pyramid anti-aliasing filtering scheme. Inspired by Refs. [15,21], classical images are represented in quantum form using the NEQR model and the INCQI model. The original image undergoes anti-aliasing filtering and blurring processes, followed by bilinear interpolation for image scaling. This process is repeated several times to construct a pyramid model, providing users with the option to select an appropriate image application. The selected image is then enlarged to its original size. Experimental results demonstrate that the proposed approach produces smoother images compared to simply scaling the images, as seen in Ref. [21].

The remaining sections of this paper are organized as follows. Section 2 introduces essential theoretical foundations, including the NEQR model, INCQI model, aliasing phenomenon, Gaussian pyramid, bilinear interpolation method, and spatial-domain image filtering algorithm. In Section 3, the core quantum modules are listed, which are used to design integrated quantum circuits capable of quantum image scaling and anti-aliasing filtering. Section 4 provides detailed anti-aliasing filtering methods and specific quantum circuits. Section 5 analyzes the circuit complexity and presents experimental results. Finally, Section 6 concludes and outlines future work.

2. Theoretical base

2.1. The quantum representation of classical images

2.1.1. A novel enhanced quantum representation of digital images (NEQR)

For a grayscale image of size $2^n \times 2^n$ with a grayscale range of 2^q, NEQR encodes positional information using $2n$ quantum bits and grayscale intensity using q quantum bits, as expressed by

$$\begin{aligned} |I\rangle &= \frac{1}{2^n}\sum_{Y=0}^{2^n-1}\sum_{X=0}^{2^n-1}|C_{YX}\rangle|YX\rangle \\ &= \frac{1}{2^n}\sum_{Y=0}^{2^n-1}\sum_{X=0}^{2^n-1}|C_{YX}^{q-1}C_{YX}^{q-2}\cdots C_{YX}^{0}\rangle|YX\rangle^{\omega}, \end{aligned} \tag{1}$$

where $|C_{YX}\rangle \in \{0,1,\ldots 2^q-1\}, C_{YX}^{q-1}, C_{YX}^{q-2}, \ldots C_{YX}^{0} \in \{0,1\}$. Figure 1 shows an example of a 4×4 gray image and its NEQR representation.

$$|I\rangle = \frac{1}{4}\begin{pmatrix} |0\rangle\otimes|0000\rangle + |20\rangle\otimes|0001\rangle + |40\rangle\otimes|0010\rangle + |60\rangle\otimes|0011\rangle \\ +|80\rangle\otimes|0100\rangle + |100\rangle\otimes|0101\rangle + |120\rangle\otimes|0110\rangle + |140\rangle\otimes|0111\rangle \\ +|150\rangle\otimes|1000\rangle + |170\rangle\otimes|1001\rangle + |200\rangle\otimes|1010\rangle + |210\rangle\otimes|1011\rangle \\ +|220\rangle\otimes|1100\rangle + |230\rangle\otimes|1101\rangle + |240\rangle\otimes|1110\rangle + |255\rangle\otimes|1111\rangle \end{pmatrix}$$

$$= \frac{1}{4}\begin{pmatrix} |000000000\rangle \otimes |0000\rangle + |00010100\rangle \otimes |0001\rangle + |00101000\rangle \otimes |0010\rangle + |00111100\rangle \otimes |0011\rangle \\ +|01010000\rangle \otimes |0100\rangle + |01100100\rangle \otimes |0101\rangle + |01111000\rangle \otimes |0110\rangle + |010001100\rangle \otimes |0111\rangle \\ +|10010110\rangle \otimes |1000\rangle + |10101010\rangle \otimes |1001\rangle + |11001000\rangle \otimes |1010\rangle + |11010010\rangle \otimes |1011\rangle \\ +|11011100\rangle \otimes |1100\rangle + |11100110\rangle \otimes |1101\rangle + |11110000\rangle \otimes |1110\rangle + |11111111\rangle \otimes |1111\rangle \end{pmatrix}. \quad (2)$$

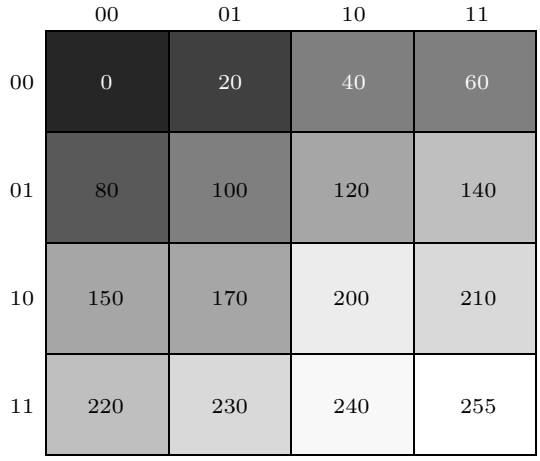


Fig. 1. An example of a 4×4 gray image and its NEQR representation.

2.1.2. A novel quantum representation of color digital images (NCQI)

In 2016, Sang *et al.* introduced an innovative quantum representation method for color digital images in their research, known as the NCQI.[44] For a color digital image of size $2^n \times 2^n$, its NCQI representation can be given as follows:

$$|I\rangle = \frac{1}{2^n}\sum_{Y=0}^{2^n-1}\sum_{X=0}^{2^n-1}|C(Y,X)\rangle \otimes |YX\rangle. \quad (3)$$

In this representation, $|Y\rangle$ and $|X\rangle$ represent the vertical and horizontal coordinates of the respective position. Meanwhile, $|C(Y,X)\rangle$ denotes the pixel value information at the corresponding position, which can be encoded using the following binary sequence:

$$\begin{aligned} |C(Y,X)\rangle &= |R(Y,X)G(Y,X)B(Y,X)\rangle \\ &= |\underbrace{R_{q-1}\ldots R_0}_{\text{Red}}\underbrace{G_{q-1}\ldots G_0}_{\text{Green}}\underbrace{B_{q-1}\ldots B_0}_{\text{Blue}}\rangle. \end{aligned} \quad (4)$$

The values for each channel (R, G, B) are constrained within the range. Equation (2) indicates that the entire NCQI model is stored in a normalized quantum superposition state. For the three channels (R, G, B) of a pixel, the NCQI model for a quantum color image consists of three parts: $|C(Y,X)\rangle$ representing color information, $|Y\rangle$ representing vertical positional information, and $|x\rangle$ representing horizontal positional information. According to the equation, $2n+3q$ quantum bits are employed to store a $2^n \times 2^n$ quantum color digital image, with each channel (R, G, B) constrained within the range $[0, 2^q-1]$ and mapped to the NCQI state.

2.1.3. Improved NCQI model (INCQI)

When performing scaling operations on images, the original NCQI model, designed for representing images of size $2^n \times 2^n$, cannot be directly applied when dealing with different two-dimensional scaling ratios. To address this issue, Zhou *et al.* proposed an enhanced NCQI model (referred to as the INCQI)[17] in their research to represent quantum images with pixel dimensions of $2^{n_1} \times 2^{n_2}$. In the following we provide a description of this improvement:

$$|I\rangle = \frac{1}{2^{\frac{n_1+n_2}{2}}}\sum_{Y=0}^{2^{n_1}-1}\sum_{X=0}^{2^{n_2}-1}|C(Y,X)\rangle|YX\rangle. \quad (5)$$

The INCQI model employs distinct numbers of quantum bits to represent the Y-coordinate (using n_1 quantum bits), X-coordinate (using n_2 quantum bits), and pixel values (using $3q$ quantum bits) of a quantum color image. Figure 2 provides a straightforward example, illustrating an INCQI color image with dimensions 4×2 along with its corresponding quantum representation:

$$|I\rangle = \frac{1}{\sqrt{2^3}} \cdot \begin{bmatrix} |\underbrace{11111111}_{\text{Red}}\underbrace{00000000}_{\text{Green}}\underbrace{00000000}_{\text{Blue}}\rangle \otimes (|000\rangle + |001\rangle) \\ +|\underbrace{00000000}_{\text{Red}}\underbrace{11111111}_{\text{Green}}\underbrace{00000000}_{\text{Blue}}\rangle \otimes (|010\rangle + |011\rangle) \\ +|\underbrace{00000000}_{\text{Red}}\underbrace{00000000}_{\text{Creen}}\underbrace{11111111}_{\text{Blue}}\rangle \otimes (|100\rangle + |101\rangle) \\ +|\underbrace{11111111}_{\text{Red}}\underbrace{11111111}_{\text{Green}}\underbrace{11111111}_{\text{Blue}}\rangle \otimes (|110\rangle + |111\rangle) \end{bmatrix}. \quad (6)$$

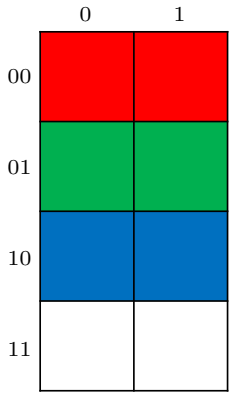


Fig. 2. An example of a 4×2 color image and its INCQI expression.

2.2. Image aliasing

Let us start by introducing the Nyquist sampling theorem, also known as the Nyquist–Shannon sampling theorem, a fundamental principle in the field of signal processing that outlines the minimum requirements for sampling in digital signals. Its development can be traced back to the early 20th

century and has undergone contributions and evolution from several scientists.

For $F_s \geq 2F_{max}$, if the aforementioned sampling conditions are not met, the sampled signal frequencies will undergo aliasing, meaning that the frequency components above half of the sampling frequency will be folded back and reconstructed as signals below half of the sampling frequency. Due to this overlap in the spectrum, the distortion caused is known as aliasing. Simultaneously, aliasing gives rise to aliasing artifacts, as these two signals share identical sample values.

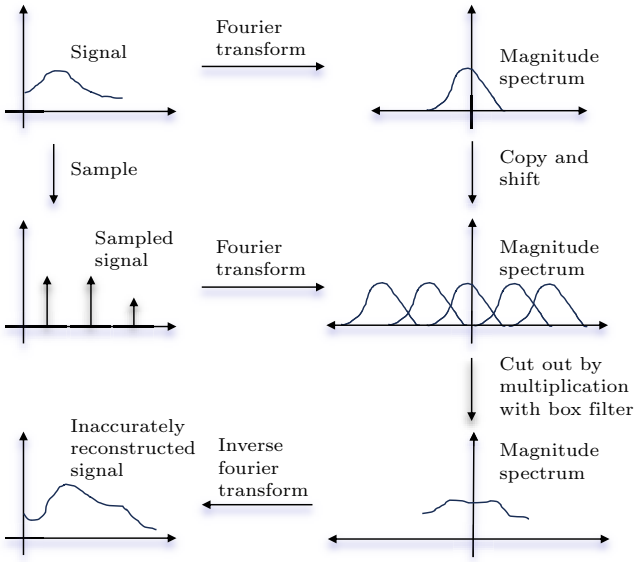


Fig. 3. Discrete signal spectrum signal overlap distortion.

If the highest frequency component F_{max} in the original signal exceeds half of the sampling frequency ($F_s/2$), the spectra of corresponding periods in the discrete signal will overlap, resulting in distortion in the eventually reconstructed analog signal, as shown in Fig. 3.

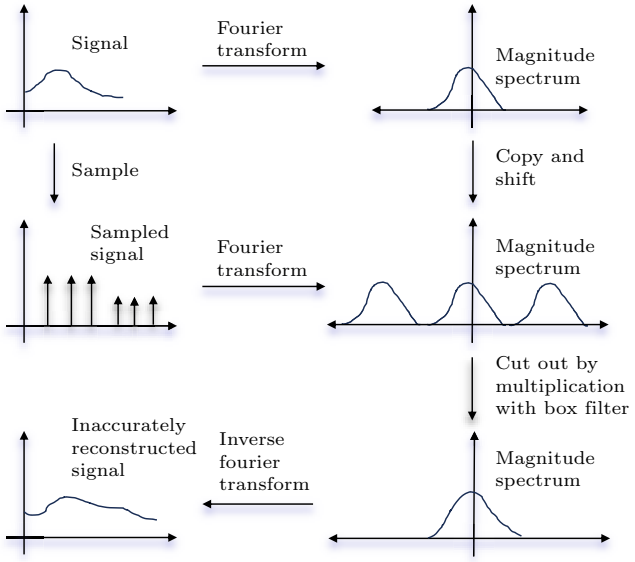


Fig. 4. The discrete signal spectrum signal is not overlapped and undistorted.

Conversely, if $F_{max} < F_s/2$, meaning that the sampling frequency is greater than twice the highest frequency component in the analyzed signal, there will be no frequency aliasing in the discrete signal spectrum after sampling, as illustrated in Fig. 4.

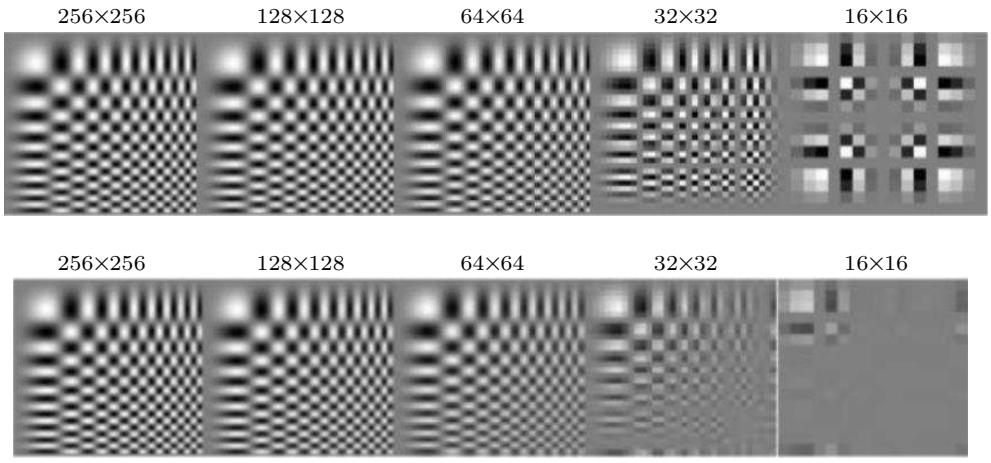


Fig. 5. Comparison between two identical signals, one with Gaussian filtering applied and the other without.

A sinusoidal wave with a frequency exactly half of the sampling frequency typically aliases into another sinusoidal wave with the same frequency but altered phase and amplitude. Two measures can prevent aliasing: (1) Increase the sampling frequency to more than twice the highest frequency. (2) Introduce a low-pass filter.

In Fig. 5, the upper row represents unsampled data, and distortion becomes apparent in the later stages. The lower row, on the other hand, illustrates down-sampling with Gaussian filtering, where although there is some data loss, distortion does not occur.

The Gaussian pyramid involves the incorporation of a

Gaussian filter as a low-pass filter, thereby suppressing high-frequency components to prevent aliasing and avoid distortion in the down-sampled image.

2.3. Gaussian pyramid model

The Gaussian pyramid is a multiscale representation technique widely used in image processing and computer vision. Its purpose is to effectively handle different scale information in images. It is extensively employed in various fields such as feature extraction, edge detection, and object recognition, enabling the analysis of image features at different scales. In this study, the Gaussian pyramid model is applied to image anti-aliasing filtering, effectively preventing aliasing issues that commonly occur during image scaling.

The construction of the Gaussian pyramid relies on image blurring and subsampling operations. Initially, the original image undergoes blurring by applying a series of Gaussian filters, each corresponding to a different scale. The convolution operation of these filters gradually reduces high-frequency details in the image, resulting in a somewhat blurred image. Subsequently, the blurred image is subsampled to obtain a smaller-sized image, referred to as the next layer of the pyramid. This process is repeated, each time using different-scale Gaussian filters and subsampling operations, to construct multiple layers of the pyramid.

The Gaussian pyramid provides a multiscale representation of images, allowing the observation of image features at different levels. At lower levels, image details are clearer, while at higher levels, overall image features become more prominent. This multiscale representation aids in detecting objects, extracting features, and overcoming scale variations in images.

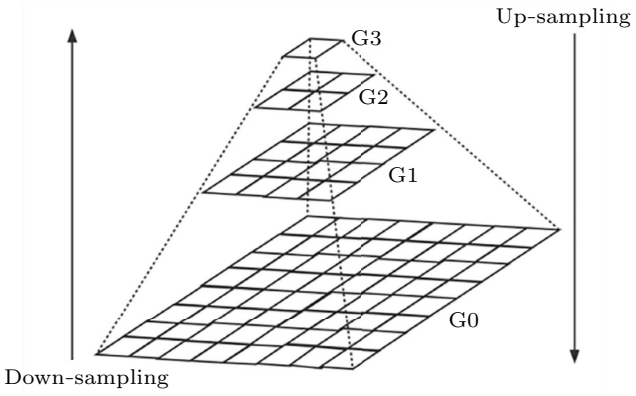


Fig. 6. Schematic diagram of up-sampling and down-sampling in the pyramid model.

As shown in Fig. 6, the image consists of four layers, representing the layers as a pyramid. It can be obtained through a down-sampling process layer by layer until a specific termination condition is met. However, during the down-sampling process, as the levels increase, pixel sizes decrease, leading to a reduction in clarity. The generation of an image pyramid mainly involves two methods: down-sampling and up-sampling. Down-sampling transforms the image from G0 to G1, G2, G3, gradually decreasing the image's clarity. On the other hand, up-sampling transforms the image from G3 to G2, G1, G0, enhancing the image's clarity.

2.3.1. Downsampling/subsampling

This process generally involves two steps: (1) Applying a Gaussian convolution kernel (Gaussian filtering) to the image. (2) Removing all even rows and columns.

Here, we assume two rounds of filtering on the image, resulting in an image with only one-fourth of the original pixel count. By iteratively applying these steps to the input image (original image), the entire pyramid is obtained. However, downsampling gradually leads to the loss of image information.

2.3.2. Upsampling/up-sampling

This process generally involves two steps: (1) Enlarging the image in each direction to twice its original size, adding rows and columns filled with zeros. (2) Using bilinear interpolation: first, interpolate by averaging along rows, and then interpolate by averaging along columns.

2.4. Bilinear interpolation amplification method

In the traditional image scaling process, no matter whether it is enlargement or reduction, interpolation methods are commonly used. Interpolation aims to adjust digital images by generating new pixels or eliminating redundant pixels. The commonly used interpolation methods include nearest-neighbor interpolation, bilinear interpolation, and bicubic interpolation. In this work, we utilize the bilinear interpolation method from Refs. [16,17] for both grayscale and color image scaling. Since the steps for grayscale images are simpler, we only provide the specific experimental steps for quantum color images here. The quantum modules in 3 will also present steps for color images, while 5 will present the results for grayscale images in the experiments.

Bilinear interpolation is typically applied in the two-dimensional case of images, encompassing both vertical and horizontal directions. Its corresponding functional expression is

$$I' = f(I,a,b) = f_y(f_x(I,a),b) = f_x(f_y(I,b),a). \quad (7)$$

Here, I represents the original image, I' denotes the scaled image, f is the scaling function, and a and b represent the vertical and horizontal scaling ratios, respectively. The function f can be decomposed into f_y and f_x, corresponding to the vertical and horizontal scaling functions. The principles of f_y and f_x are identical, allowing them to be interchangeable. In simpler terms, they can freely determine the order of vertical and

horizontal operations. Therefore, regardless of whether we initially perform scaling in the vertical or horizontal dimension, the final result of the scaled image will be exactly the same.

In this paper, we adopt a color image $|I\rangle$ with dimensions of $2^{n_1} \times 2^{n_2}$, represented using the INCQI model. The color depth for each RGB channel is q. Therefore, the color information of the image $|I\rangle$ and its positional information need to be represented by $3q$ quantum bits and (n_1+n_2) quantum bits, respectively.

2.4.1. Quantum color image reduction scheme

In this scenario, we explore a quantum color image reduction scheme based on the INCQI model. Suppose we want to scale down a color image of size $2^{n_1} \times 2^{n_2}$ to an image of size $2^{n_1-j} \times 2^{n_2-k}$, where n_1, n_2, j, and k are all non-negative integers. In this case, the vertical and horizontal scaling ratios are given by $a = 2^{-j}$ and $b = 2^{-k}$. Based on the properties of image sizes, we can ascertain that $n_1 > j$ and $n_1 > k$.

With the help of bilinear interpolation, we can obtain the color value $|C_{D',C'}\rangle$ at the location (D',C') in the interpolated image $|I'\rangle$ corresponding to the four coordinates of the original image $|I\rangle$. Through equivalent substitution, the interpolated pixel value $|C_{D',C'}\rangle$ can be expressed as

$$
\begin{aligned}
|C_{D',C'}\rangle &= (1-b)(1-a)|C_{D,C}\rangle + (1-b)a|C_{D,C+1}\rangle \\
&\quad + b(1-a)|C_{D+1,C} > + ab|C_{D+1,C+1}\rangle \\
&= \left[1-\left(\frac{D'}{2^{-j}} - D\right)\right] \times \left[1-\left(\frac{C'}{2^{-k}} - C\right)\right] \times |C_{D,C}\rangle \\
&\quad + \left[1-\left(\frac{D'}{2^{-j}} - D\right)\right] \times \left(\frac{C'}{2^{-k}} - C\right) \times |C_{D,C+1}\rangle \\
&\quad + \left(\frac{D'}{2^{-j}} - D\right) \times \left[1-\left(\frac{C'}{2^{-k}} - C\right)\right] \times |C_{D+1,C}\rangle \\
&\quad + \left(\frac{D'}{2^{-j}} - D\right) \times \left(\frac{C'}{2^{-k}} - C\right) \times |C_{D+1,C+1}\rangle \\
&= \left[1-\left(D' \times 2^{j} - D' \times \frac{2^{n_1}}{2^{n_1-j}}\right)\right] \\
&\quad \times \left[1-\left(c' \times 2^{k} - c' \times \frac{2^{h_r}}{2^{h_r-\bar{k}}}\right)\right] \times |C_{D,C}\rangle \\
&\quad + \left[1-\left(D' \times 2^{j} - D' \times \frac{2^{n1}}{2^{n_1-j}}\right)\right] \\
&\quad \times \left(C' \times 2^{k} - C' \times \frac{2^{n_2}}{2^{n_2-k}}\right) \times |C_{D,C+1}\rangle \\
&\quad + \left(D' \times 2^{j} - D' \times \frac{2^{n_1}}{2^{n_1-j}}\right) \\
&\quad \times \left[1-\left(C' \times 2^{k} - C' \times \frac{2^{n_2}}{2^{n_2-k}}\right)\right] \times |C_{D+1,C}\rangle \\
&\quad + \left(D' \times 2^{j} - D' \times \frac{2^{n_1}}{2^{n_1-j}}\right) \\
&\quad \times \left(C' \times 2^{k} - c' \times \frac{2^{n_2}}{2^{n_2-\bar{k}}}\right) \times |C_{D+1,C+1}\rangle \\
&= |C_{D,C}\rangle. \qquad (8)
\end{aligned}
$$

From the above formula, it can be observed that the pixel value $|C_{D',C'}\rangle$ at the location (D',C') in the interpolated image $|I'\rangle$ is ultimately determined by the pixel value $|C_{D,C}\rangle$ at the location (Y,X) in the original image $|I\rangle$. Therefore, in this case, the interpolation algorithm used is slightly different from the traditional bilinear interpolation. The specific circuit diagram for this scheme is shown in Fig. 7 and will be utilized as the quantum color circuit reduction module in the subsequent experiments in Section 3.

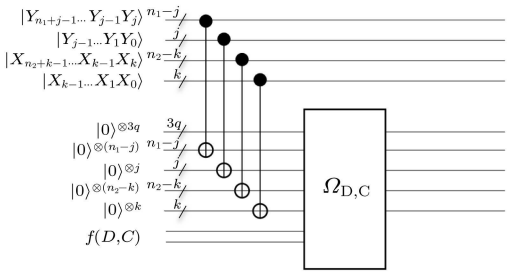


Fig. 7. The schematic diagram of up-sampling and down-sampling in the pyramid model.

2.4.2. Quantum color image enlargement scheme

Similar to the aforementioned reduction scheme, suppose we want to scale up a color image of size $2^{n_1} \times 2^{n_2}$ to an image of size $2^{n_1+j} \times 2^{n_2+k}$, where n_1, n_2, j, and k are all non-negative integers. In this case, the vertical and horizontal scaling ratios are given by $a = 2^{j}$ and $b = 2^{k}$. Omitting the corresponding calculation steps, for those we are interested in, the specific circuit is shown in Fig. 8.

2.5. Quantum multiplier

Before performing operations such as edge detection and segmentation, it is common to use image filtering as a preprocessing stage to eliminate noise. One common method involves applying a filter function to the image through correlation or convolution. However, Lomont[41] demonstrated that quantum correlation and convolution of two sequences are impossible to achieve. This is because it is not possible to perform multiplication steps subject to linear constraints.

In 2016, Yuan *et al.* proposed a quantum image filtering algorithm in spatial domain, cleverly using quantum addition instead of quantum multiplication for correlation operations, and ultimately succeeded in experimentation.[42] However, a few months later, some flaws were pointed out: (1) The exact values of the filter coefficients need to be known before each filtering operation. (2) This method is only applicable to integer filter coefficients, not decimal filter coefficients.

Subsequently, in 2017 Yuan *et al.* introduced an improved spatial domain quantum image filtering algorithm in Ref. [43]. In the referenced literature,[42] they used quantum fake gates instead of quantum multiplication, while in the improved version, they designed a quantum multiplier based on quantum addition. In quantum multiplication operations, solving the mentioned problems only requires one additional quantum operation compared to designing quantum addition operations,

namely the quantum right shift operation. The structure of the multiplier is shown in Fig. 9.

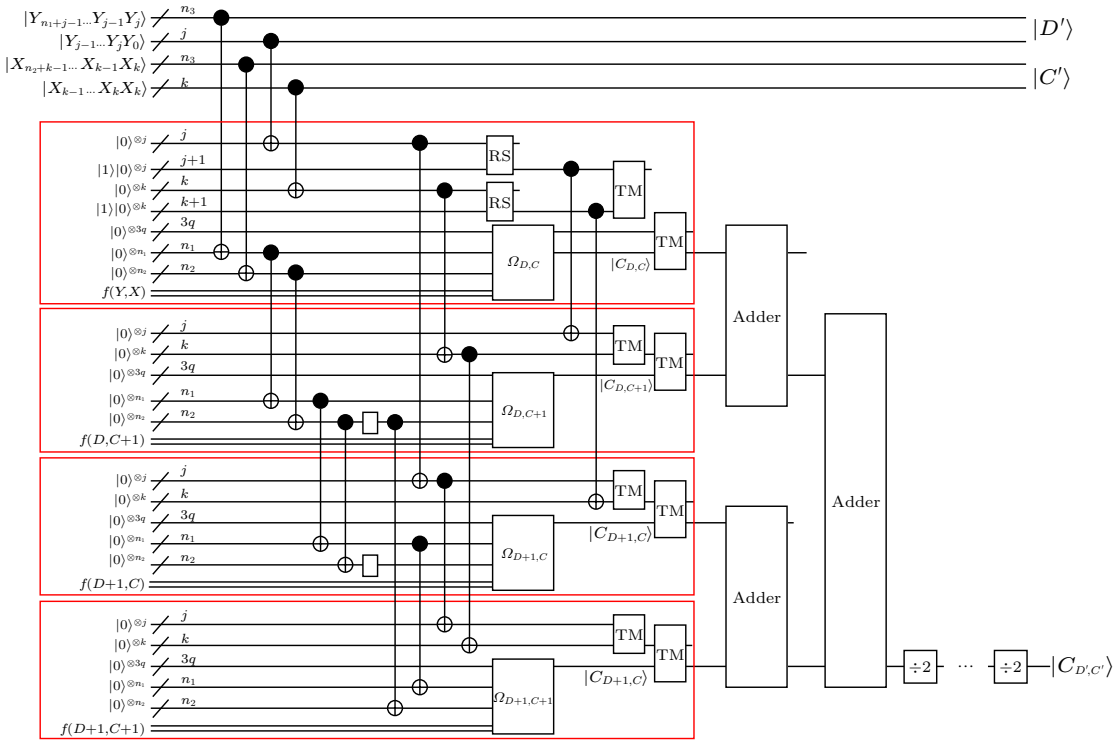


Fig. 8. Quantum color image enlargement circuit.

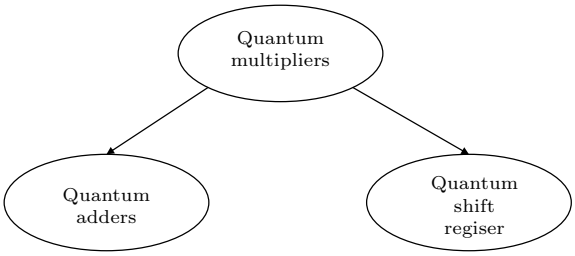


Fig. 9. Composition of quantum multipliers.

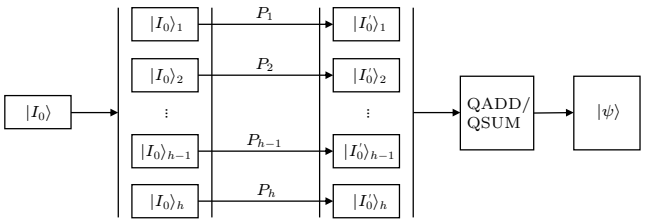


Fig. 10. Quantum circuit of quantum image filtering.

Here the quantum version of the original image is duplicated h times, and the operation of obtaining the neighborhood image set through position shift transformation remains unchanged. The improvement lies solely in the QADD/QSUM steps, using convolution operation to obtain the filtered image.

The key steps can be summarized in the following three steps:

(1) Prepare $(2k+1)\times(2k+1)$ identical quantum images

The specific workflow of the non-improved version is illustrated in Fig. 10, as described in the following.

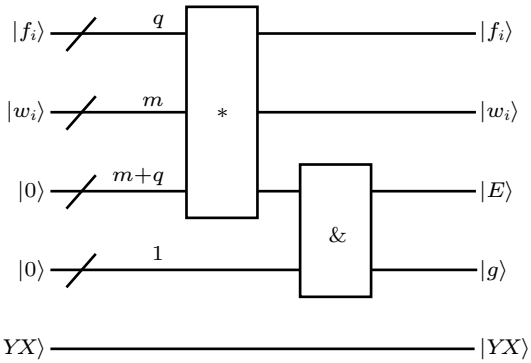


Fig. 11. Quantum convolution. Only once addition and multiplication are realized, which needs to be implemented W times to complete the whole convolution.

$|I_{YX}\rangle$, and these copies of $|I_{YX}\rangle$ can be represented as

$$\{|I_{YX}\rangle_1, |I_{YX}\rangle_2, \ldots, |I_{YX}\rangle_{(2k+1)\times(2k+1)}\}.$$

(2) Perform position displacement operations on the $(2k+1)\times(2k+1)$ copies of quantum images obtained in step 1, and we can obtain the neighborhood image set, expressed as

$$\{|I_{Y-k,X-k}\rangle, |I_{Y-k,X-k+1}\rangle, \ldots, |I_{Y,X}\rangle, \ldots, |I_{Y+k,X+k-1}\rangle, |I_{Y+k,X+k}\rangle\}.$$

(3) Compute the convolution result. By applying quantum full-adder and multiplier operations, we can design a quantum circuit as shown in the figure to store the result of the convolution

in $|g(Y,X)\rangle$. Ignoring auxiliary quantum bits, we can obtain the following result:

$$|I\rangle = \frac{1}{2^n}\sum_{Y=0}^{2^n-1}\sum_{X=0}^{2^n-1}|g(Y,X)\rangle|YX\rangle.$$

The specific process is illustrated in Fig. 11.

3. Quantum modules

In this section, we provide a brief overview of the series of quantum modules used in the proposed quantum color image scaling circuit. These modules include the quantum right shift operator module, multiplier module, adder module,[21] quantum color image reduction module, quantum color image enlargement module, and the anti-aliasing downsampling (Aad) module.

3.1. Right shift operator module

Analogous to binary multiplication, as long as we continuously perform multiplication and right shift on each bit of the multiplier and multiplicand, and then summing up all the results, we can obtain the multiplication result. In quantum computing, multiplication as a computation can be avoided. As shown in Fig. 12, we can use two CNOT gates to perform a swap operation on two quantum bits.

After performing n iterations of this operation, we can achieve a right shift effect, as illustrated in Fig. 13.

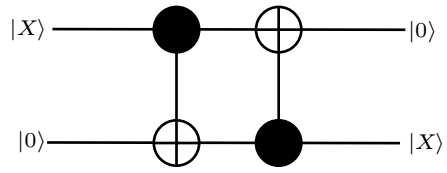


Fig. 12. To exchange two quantum bits, two CNOT gates can be utilized, with one of them required to be the $|0\rangle$.

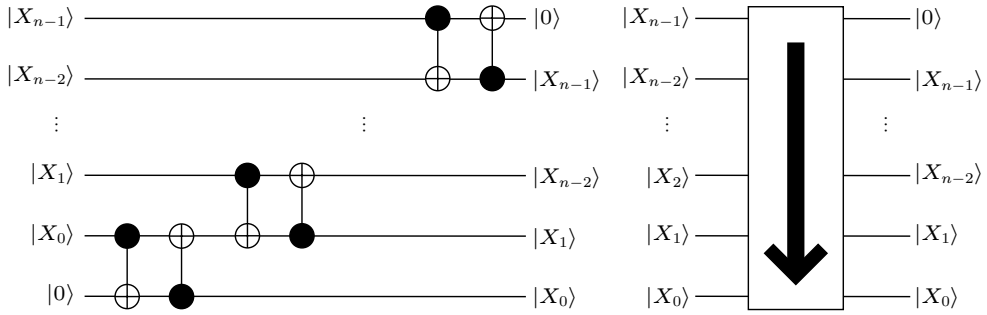


Fig. 13. Right shift operator module and simplified right shift operator module.

3.2. Quantum multiplier module

Referring to Ref. [19], this module combines the quantum full adder module and the right shift operator module to achieve the effect of multiplication. As shown in Fig. 14, the multiplier is an m-bit quantum sequence $|b\rangle$, the multiplicand is an n-bit quantum sequence $|a\rangle$, and $|E_n\rangle$ is the carry of the quantum full adder. The final result is stored in $m+n$ quantum bits. Figure 15 illustrates the simplified quantum multiplier.

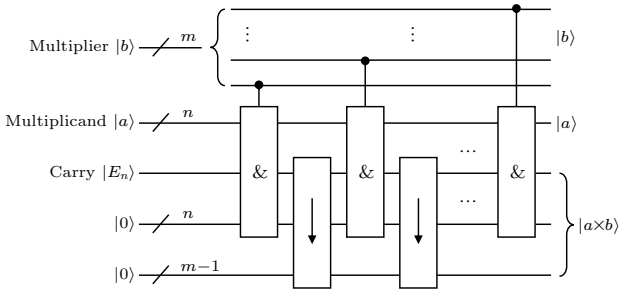


Fig. 14. Quantum multiplier. The quantum gate with a sign is an n-bit quantum adder.

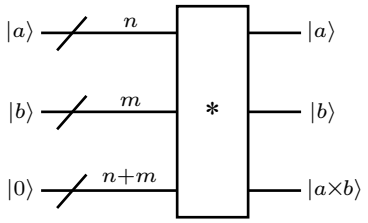


Fig. 15. Simplified quantum multiplier.

3.3. Quantum color image downsizing module

The quantum color image reduction module can proportionally shrink a color image of size $2^{n_1}\times 2^{n_2}$, ultimately resulting in a color image of size $2^{n_1-j}\times 2^{n_2-k}$. The detailed circuit diagram is shown in Fig. 7, with its simplified model depicted in the following diagram.

3.4. Quantum color image magnification module

Similarly to Subsection 3.3, we encapsulate the operation of enlarging a $2^{n_1}\times 2^{n_2}$ colored image into a module for ease of practical use. The specific circuit diagram is shown in Fig. 8, and a brief circuit diagram is provided here.

3.5. Adder module

In Ref. [16], a more efficient adder module was proposed, as illustrated in Fig. 18. The purpose of the adder module is

to add n quantum bits X and n quantum bits Y using the quantum fourier transform (QFT).[20] The corresponding quantum circuit for the adder module is shown in the figure and can be decomposed into three steps: QFT, rotation module, and inverse quantum fourier transform (IQFT). To achieve addition functionality, the adder module requires only one auxiliary quantum bit. Compared to the reversible parallel adder in Ref. [21], it enhances computational performance.

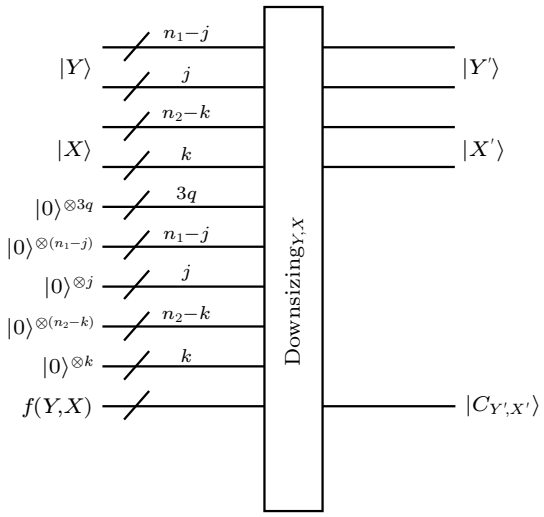


Fig. 16. Simplified quantum color image reduction module.

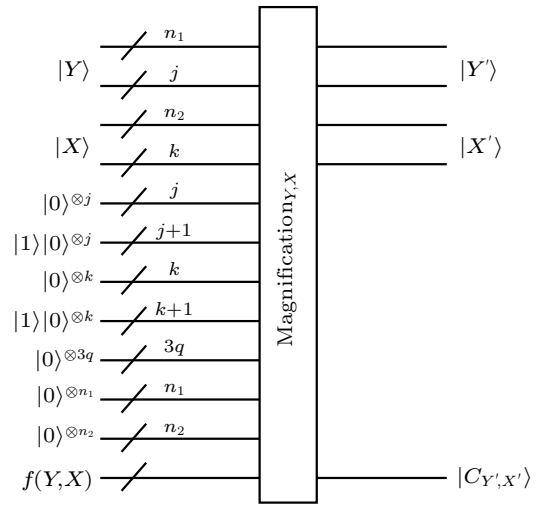


Fig. 17. Simplified quantum color image magnification module.

3.6. Anti-aliasing downsizing (Aad) module

The Aad module initially applies anti-aliasing filtering to the image and subsequently proportionally reduces the filtered image. As revealed by the workflow of the pyramid model, both filtering and downsizing operations require iterative repetitions. Therefore, in this context, we opt to organically integrate these two modules and present specific circuitry along with a simplified version. The implementation of the quantum circuit involves the previously mentioned quantum multiplication module, adder module, and quantum color image downsizing module. The simplified circuit diagram is depicted in Fig. 19.

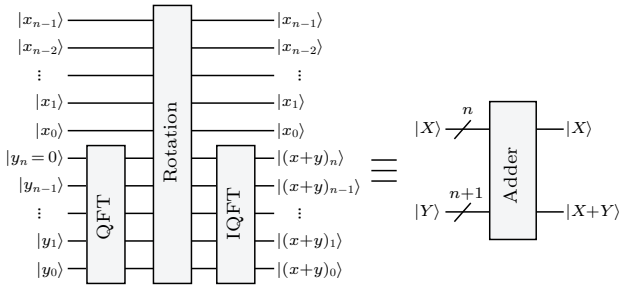


Fig. 18. Quantum circuit of adder module figure.

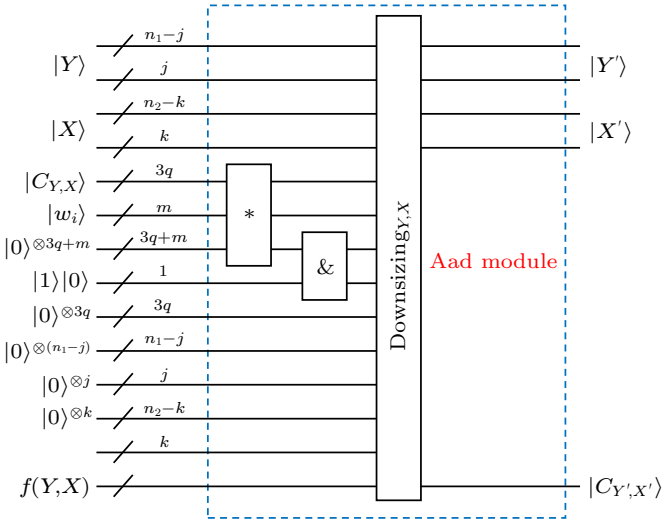


Fig. 19. The anti-aliasing downsizing (Aad) module.

4. Spatial domain quantum color image pyramid anti-aliasing filtering

In this section, we extensively discuss the application of Gaussian filters to the quantum version of the original image for anti-aliasing downsizing, followed by the creation of an image pyramid model. We propose a novel anti-aliasing downsizing module, abbreviated as the Aad module, designed for the specific case of color images. Assume that the $2^{n_1} \times 2^{n_2}$ color image $|I\rangle$ is represented by the INCQI model. Maintaining generality, the approach employs a 3×3 filtering window. Firstly, we outline the workflow of this approach. Subsequently, a detailed description and step-wise design of the circuit are provided. Finally, a comprehensive quantum circuit design is presented.

4.1. Scheme workflow

For this approach, the initial step involves converting the original image into a quantum version based on the INCQI model. Subsequently, the image is asymmetrically downsized into several portions using bilinear interpolation. Following this, quantum adder modules and displacement transformation

modules apply spatial domain Gaussian filtering to the corresponding downsized image portions multiple times, producing filtered images arranged in a pyramid model. Finally, the downsized and filtered images are enlarged back to the original size using bilinear interpolation. The workflow of this approach is depicted in Fig. 20.

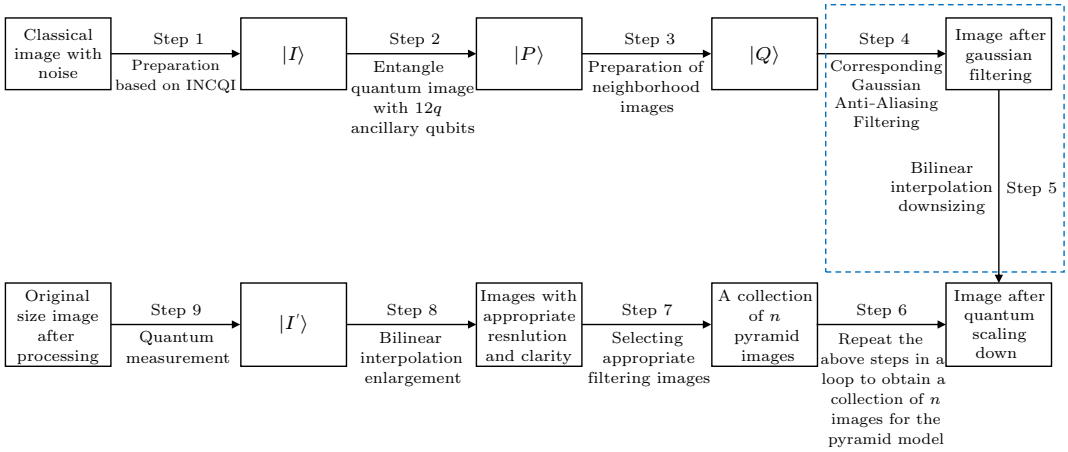


Fig. 20. Spatial domain quantum color image pyramid anti-aliasing filtering workflow.

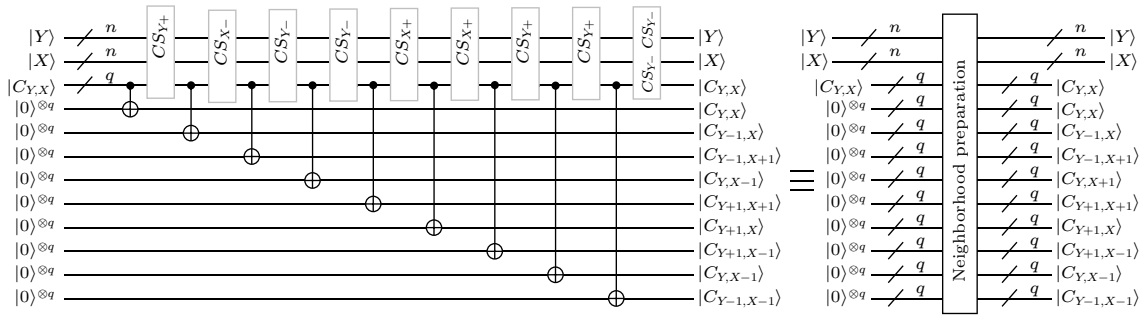


Fig. 21. Quantum circuit for the preparation of the ancillary qubits.

4.2. Step-by-step description of the algorithm

Here, we provide a more detailed explanation of the proposed approach in Fig. 19. The proposed scheme can be divided into the following seven steps:

Step 1 We convert the noisy color image to its quantum version $|I\rangle$ based on INCQI, encoding the grayscale values into eight qubits, denoted as $|C_{YX}\rangle = \bigotimes_{i=0}^{7} |C_{YX}^{i}\rangle$. The INCQI expression for the color image of size $2^{n_1} \times 2^{n_2}$ is written as

$$\begin{aligned} |I\rangle &= \frac{1}{2^n} \sum_{Y=0}^{2^{n1}-1} \sum_{X=0}^{2^{n2}-1} |C_{YX}\rangle |YX\rangle \\ &= \frac{1}{2^n} \sum_{Y=0}^{2^{n1}-1} \sum_{X=0}^{2^{n2}-1} |C_{YX}^{7} C_{YX}^{6} \cdots C_{YX}^{0}\rangle |YX\rangle, \end{aligned} \tag{9}$$

where $|YX\rangle = |y_{n-1}y_{n-2}\cdots y_1 y_0\rangle\ |x_{n-1}x_{n-2}\cdots x_1 x_0\rangle, y_i, x_i \in \{0,1\}$, the first n qubits $|y_{n-1}y_{n-2}\cdots y_1 y_0|$ encode the vertical coordinates, and the second n qubits $|x_{n-1}x_{n-2}\cdots x_1 x_0\rangle$ encode the horizontal coordinates.

Step 2 Prepare 9 auxiliary qubit sequences $|0\rangle^{\otimes q}$ to store neighborhood pixels. To fully leverage the parallelism of quantum computing, the auxiliary qubits are given by the tensor product with the state of the original quantum image, represented as follows:

$$\begin{aligned} |P\rangle = |0\rangle^{\otimes 9q} \otimes |I\rangle &= \frac{1}{2^n} \sum_{Y=0}^{2^{n1}-1} \sum_{X=0}^{2^{n2}-1} |C_{YX}\rangle |YX\rangle \\ &= \frac{1}{2^n} \sum_{Y=0}^{2^{n1}-1} \sum_{X=0}^{2^{n2}-1} |0\rangle^{\otimes q} \ldots |0\rangle^{\otimes q} |C_{YX}\rangle |YX\rangle. \end{aligned} \tag{10}$$

Step 3 Through a series of shift operations and parallel-controlled NOT (CNOT) gates on the original quantum image, we prepare 9 auxiliary qubits with neighborhood pixel values. Initially, we use 10 shift modules to obtain the pixel values in the neighborhood. Subsequently, we utilize 9 parallel-controlled NOT modules to encode these pixel values into qubit sequences. We summarize this intricate process into a complete module called the neighborhood image preparation module, and the resulting image is represented by Eq. (9). The corresponding quantum circuit design is illustrated in Fig. 21.

$$\begin{aligned} |Q\rangle = \frac{1}{2^n} \sum_{Y=0}^{2^{n1}-1} \sum_{X=0}^{2^{n2}-1} &|C_{Y-1,X}\rangle \otimes |C_{Y-1,X+1}\rangle \otimes |C_{Y,X+1}\rangle \\ &\otimes |C_{Y+1,X+1}\rangle \otimes |C_{Y+1,X}\rangle \otimes |C_{Y+1,X+1}\rangle \otimes |C_{Y,X-1}\rangle \end{aligned}$$

$$\otimes|C_{Y-1,X-1}\rangle\otimes|C_{Y,X}\rangle\otimes|C_{Y,X}\rangle|Y\rangle|X\rangle, \tag{11}$$

where $|C_{Y-1,X}\rangle$, $|C_{Y-1,X+1}\rangle$, $|C_{Y,X+1}\rangle$, $|C_{Y+1,X+1}\rangle$, $|C_{Y+1,X-1}\rangle$, $|C_{Y,X-1}\rangle$, $|C_{Y-1,X-1}\rangle$, $|C_{Y,X}\rangle$ stores the 9 neighborhood images of $|C_{Y,X}\rangle$.

Step 4 In this step, we apply the Aad module to perform the anti-aliasing filtering on the 9 neighborhood images obtained in the previous step. The operation involves convolving the absolute values of pixel values in the neighborhood images with the absolute values of corresponding filter weights (quantum adder + right shift operator). The result is the pixel value of the target pixel. This process is repeated for all points in the image, producing the filtered image, which serves as the input for step 5.

Step 5 Perform quantum color image downsizing through bilinear interpolation on the received filtered image. The quantum color image downsizing module mentioned in this paper can scale the image to any desired proportion. However, since in classical image processing, the pyramid model in step 6 typically involves halving each side, here we focus on discussing a one-time doubling of the image size per round. Detailed experimental figures are presented in Section 5.

Step 6 This step is an iterative process where the neighborhood images of the image are repeatedly subjected to the operations in steps 4 and 5. This is done to achieve filtering and downsizing operations for n iterations. Subsequently, all the filtered image sets obtained are assembled into an image pyramid model, providing users with a selection of smooth images for practical applications.

Step 7 Choose a suitable image from the generated image set as the input image for step 8. Since the number of generated images is n, use the subscript k ($k\in(1,n]$) to denote the index of the selected image.

Step 8 After achieving anti-aliasing processing on the image, the default goal is to provide the user with a smoothly processed image at the original resolution. In this step, we use the quantum color image enlargement module based on bilinear interpolation, and the final output image is denoted as $|I'\rangle$.

Step 9 The final step in image processing is typically image retrieval. As is well known, quantum measurement is the only method that can convert the quantum version into a classical image, but converting a quantum image to a classical image through a single measurement remains a challenging task. However, image filtering is often used as a preprocessing stage for other image processing algorithms, such as image feature extraction and segmentation. In other words, image retrieval is not necessary after filtering. The result of the filter can be directly used as the input for the next quantum image processing algorithm. In conclusion, quantum measurement can be considered an unnecessary step. If image retrieval is required, we recommend referring to the literature,[15] which provides detailed retrieval methods.

4.3. Complete quantum circuit of the proposed scheme

According to the principles of the proposed filtering method and the algorithm description in Subsection 4.2, the complete quantum circuit is shown in Fig. 22. The circuit consists of a neighborhood preparation module, an anti-aliasing reduction (Aar) module, a quantum color image downsizing module, and a quantum color image upsizing module.

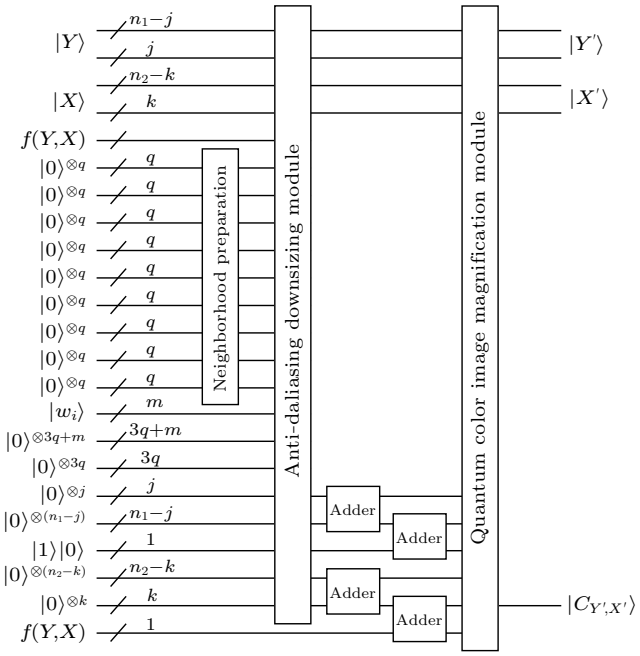


Fig. 22. Spatial domain quantum color image pyramid anti-aliasing filtering.

The output of module $|C'_{YX}|$ encodes the pixel values in the filtered image. The filtered image can be represented as

$$|I'\rangle=\frac{1}{2^n}\sum_{Y=0}^{2^{n1}-1}\sum_{X=0}^{2^{n2}-1}|\hat{C}_{YX}\rangle\,|YX\rangle. \tag{12}$$

5. Circuit complexity and simulation experiments analysis

In this section, we first delve into the circuit complexity of the proposed method. Subsequently, we present and analyze the results of simulation experiments.

5.1. Circuit complexity

In the field of quantum image processing, the complexity of the network is primarily determined by the number of basic gates used, including NOT gates, Hadamard gates, controlled NOT gates, and other basic unitary operators.[45] Here, we first analyze the complexity module by module and then calculate the overall complexity of the quantum circuit. Based on Refs. [15,17], it is evident that the preparation complexity of NEQR is $O(qn2^{2n})$, while the preparation complexity of INCQI is $O(4q+n_1+n_2+4q(n_1+n_2)\cdot 2^{n_1+n_2})$. It is important to note that the proposed algorithm can achieve anti-aliasing operations on both black and white as well as color images.

Furthermore, there are numerous methods for preparing quantum states. In this paper, we only present the anti-aliasing steps based on color images. If the preparation complexity of quantum states is included, the overall complexity will lose its generality. Therefore, we only list the complexities of the two methods before the complexity analysis but do not incorporate them into the overall experimental complexity.

(1) **Neighborhood image preparation module** As shown in the figure, 10 cyclic shift modules and 9 parallel controlled-NOT modules are used to form the neighborhood preparation module. Therefore, the complexity of this module is $O(10n^2+9q)$.

(2) **Quantum color image magnification module** This module, as known from Ref. [21], has a time complexity of $O(4(n_1+n_2+j+k)+(n_1^2+n_2^2)+4\times 3q(n_1+n_2)+(j+k)+\alpha^2+(j+k)\alpha+\alpha^2)\approx O(n_1^2+n_2^2+\alpha^2+q(n_1+n_2)+(j+k)\alpha)$, where $\alpha=\max\{3q,j,k\}$. Therefore, the time complexity of the intermediate adder module is $\mathcal{I}O(\alpha^2)$.

The time complexity of the quantum color image downsizing module, as indicated in the literature,[21] is $O((n_1-m_1)+m_1+(n_2-m_2)+m_2+3q(n_1+n_2))\approx O(q(n_1+n_2))$.

(3) According to Ref. [43], the time complexity of the multiplier and right-shift operator section can be expressed as $O(k^2(n^2+mn+q^2))$, where k is derived from the need to use $(2k+1)$ quantum multipliers and right-shift operators, m and n represent the numbers of sequences for the convolution of two quantities.

(4) **Aad module** This module consists of a quantum multiplier module, a quantum full adder module, and a quantum color image downsizing module. When calculating the product of m quantum bits and n quantum bits in binary, the complexity of the Aad module circuit can be expressed as $O(k^2(n^2+mn+q^2)+q(n_1+n_2))$. The overall circuit time complexity can be expressed as $O(14n^2+9q+k^2(n^2+mn+q^2)+q(n_1+n_2)+n_1^2+n_2^2+\alpha^2+q(n_1+n_2)(j+k)\alpha)$

Based on the above complexity analysis, it can be concluded that the complexity of our proposed anti-aliasing filtering scheme is a quadratic function with respect to image size, color depth, and the number of right shifts and additions. Since anti-aliasing filtering is performed on the basis of scaling, the complexity is relatively increased compared to Refs. [21,43], while the resulting images in the experimental stage are smoother.

5.2. Simulation experiments and analysis

Due to the absence of practical quantum computers, the simulation experiments were conducted on a classical computer with an Intel(R) Core(TM) i5-7200U CPU @ 2.70 GHz, 8.00 GB RAM, 64-bit operating system, and MATLAB 2016b. To simulate the Hilbert space, quantum states were represented using vectors, and unitary transformations were represented using unitary matrices. A detailed analysis of the experimental results is provided in the following.



Fig. 23. The original Barbara image and the experimental image subjected only to scaling.

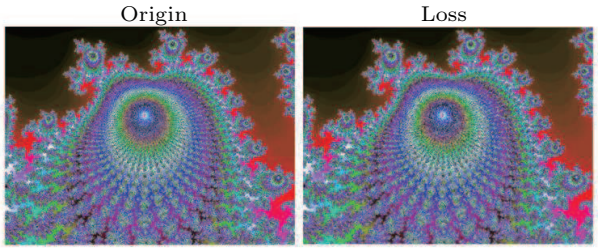


Fig. 24. The original MandelZot image and the experimental image subjected only to scaling.

In the experiment, a grayscale image named Barbara with a size of 512×512 and a color image named MandelZot with a size of 878×659 were selected. In the following experimental images, 'origin' denotes the original image, 'loss' represents the distorted image obtained only by scaling, 'first' depicts the image after a single anti-aliasing filtering operation, and 'second' signifies the image after two anti-aliasing filtering operations. Let us first take a look at the images after only undergoing scaling operations. We set the images to be scaled down by a factor of 0.5 followed by an enlargement by a factor of 2. The specific experimental images are shown in Figs. 23 and 24.

We can clearly observe significant distortion in both grayscale and color images, specifically noticeable in the prominent patterns within the images. Our proposed spatial domain pyramid anti-aliasing filtering scheme aims to mitigate the impact of aliasing artifacts on images.

Here we first apply anti-aliasing filtering to the original image by using a 3×3 low-pass filter. Subsequently, we resize the image. Repeating these two operations twice, we obtain the specific experimental images of grayscale and color images after anti-aliasing filtering, as shown in Figs. 25 and 26.

Constructing them into pyramid models separately, as shown in Figs. 27 and 28.

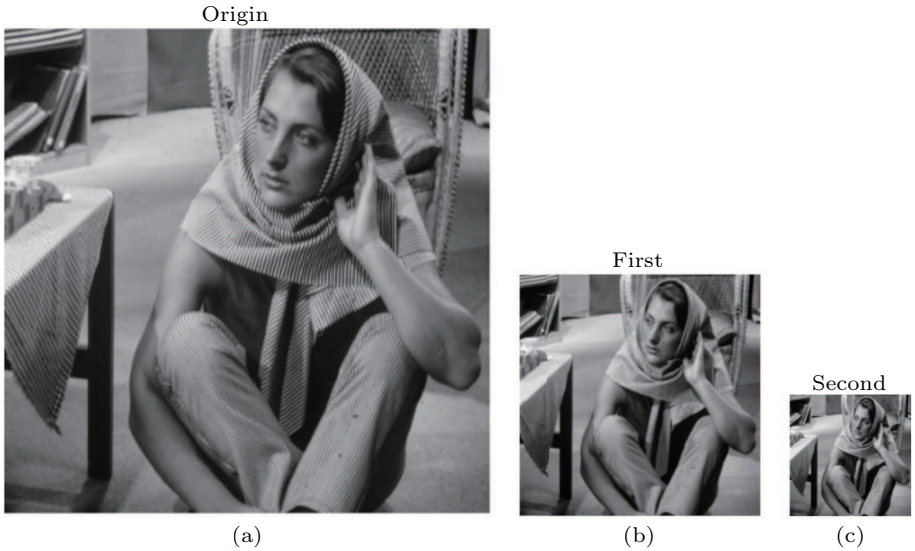


Fig. 25. (a) The Barbara original image, (b) the Barbara image after one anti-aliasing filtering operation, (c) the Barbara image after two anti-aliasing filtering operations.

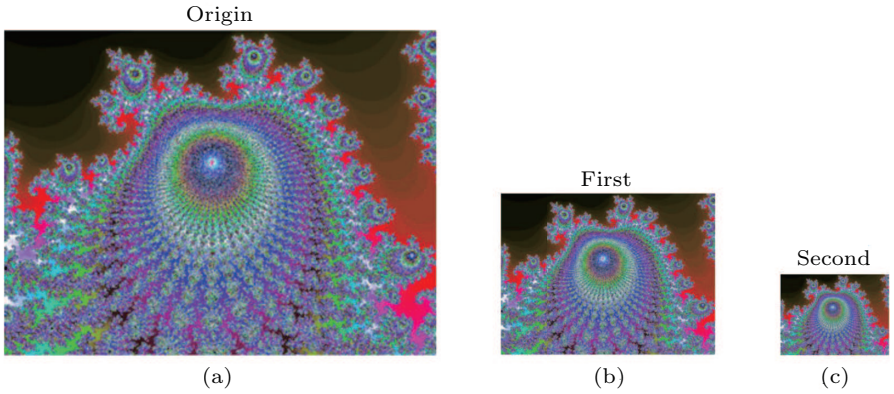


Fig. 26. (a) The MandelZot original image, (b) the MandelZot image after one anti-aliasing filtering operation, (c) the MandelZot image after two anti-aliasing filtering operations.



Fig. 27. The Barbara pyramid model.

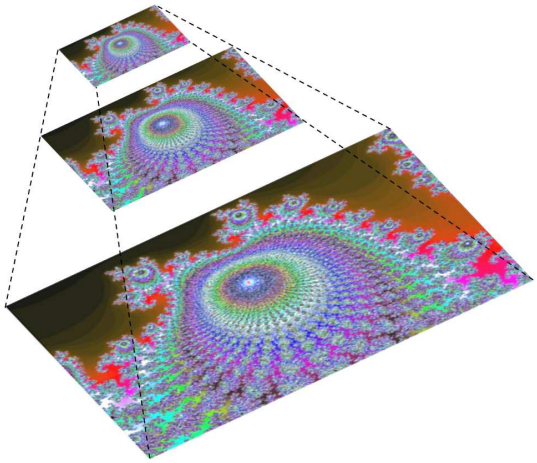


Fig. 28. The MandelZot pyramid model.

From the pyramid model, it is evident that the image after a single anti-aliasing process appears sharper and smoother. Hence, we select it as our target image for the subsequent upscaling process to restore it to the original image size, completing a full cycle.

In the end, we also display all the images at the same resolution throughout the process. It is evident that after applying anti-aliasing filtering once, the image becomes smoother and clearer, which is represented by images in Figs. 29(c) and 30(c).

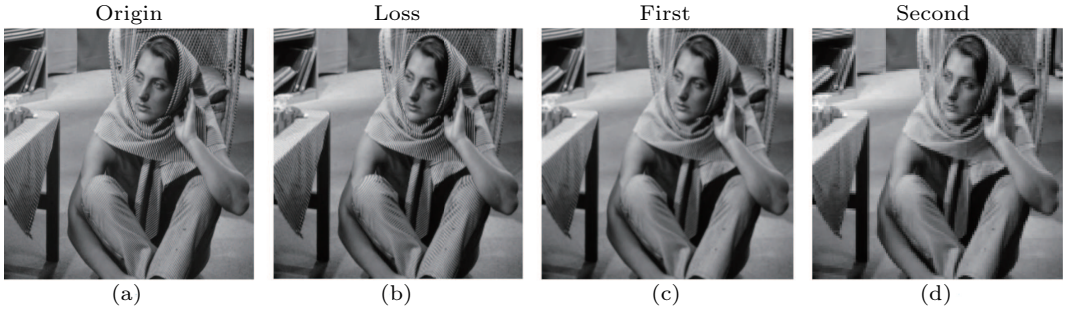


Fig. 29. (a) The Barbara original image, (b) the Barbara image with scaling only, (c) the Barbara image after applying anti-aliasing filter once, (d) the Barbara image after applying anti-aliasing filter twice.

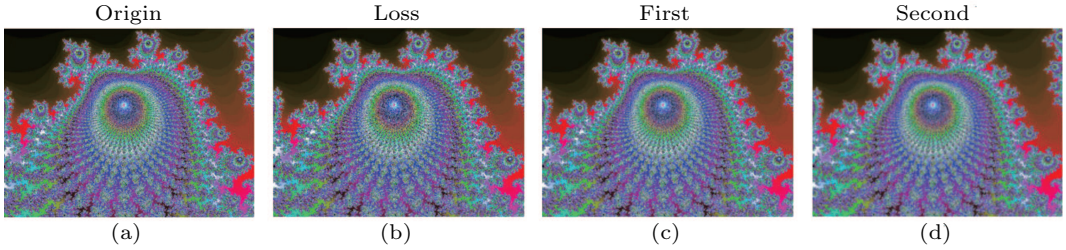


Fig. 30. (a) The MandelZot original image, (b) the MandelZot image with scaling only, (c) the MandelZot image after applying anti-aliasing filter once, (d) the MandelZot image after applying anti-aliasing filter twice.

6. Conclusion

Improvements in quantum image processing aim to advance image applications into the more sophisticated field of quantum computing by adopting classical computational methods. This paper introduces a spatial domain anti-aliasing pyramid filtering scheme based on the NEQR and INCQI models. The construction of this strategy involves two key steps: (1) combining filtering and bilinear interpolation scaling to achieve dynamic anti-aliasing filtering, and (2) applying the pyramid model to quantum image processing. Based on these two key steps, we design corresponding quantum circuits to achieve anti-aliasing filtering during quantum image downsizing. Additionally, we analyze the circuit's complexity and conduct simulation experiments to demonstrate the feasibility of this strategy.

The contributions of this paper are as follows: (1) Propose a novel quantum-level anti-aliasing processing strategy for images. (2) Cleverly apply the pyramid model in quantum image processing. (3) The introduced anti-aliasing solution exhibits lower complexity compared to classical filtering. Additionally, it is distinctly noticeable that the resulting images are smoother compared to those obtained solely through scaling in the literature.[21]

Future work will mainly include: (1) Expand the scope of this solution to achieve anti-aliasing filtering for quantum color images at arbitrary scales, as the current implementation only accomplishes integer multiples of scaling. (2) Consider the need for human intervention in selecting suitable images, incorporate a noise detection module in subsequent stages to detect aliasing phenomena, and determine whether additional anti-aliasing filtering and downsizing operations are necessary.

Acknowledgements

Project supported by the National Natural Science Foundation of China (Grant Nos. 62172268 and 62302289) and the Shanghai Science and Technology Project (Grant Nos. 21JC1402800 and 23YF1416200).

References

[1] Feynman R P 1982 *Int. J. Theor. Phys.* **21** 467
[2] Deutsch D 1985 *Proc. R. Soc. Lond. A* **400** 97
[3] Shor P W 1994 *Proceedings 35th Annual Symposium on Foundations of Computer Science*, Santa Fe, NM, USA, Nov. 20–22, 1994, pp. 124–134
[4] Grover L K 1996 arXiv:quant-ph/9605043
[5] Cong I, Choi S and Lukin M D 2019 *Nat. Phys.* **15** 1273
[6] Li Y, Zhou R G, Xu R, Luo J and Hu W 2020 *Quantum Sci. Technol.* **5** 044003
[7] Henderson M, Shakya S, Pradhan S and Cook T 2020 *Quantum Mach. Intell.* **2** 2
[8] Zhou M G, Cao X Y, Lu Y S, Wang Y, Bao Y, Jia Z Y, Fu Y, Yin H L and Chen Z B 2022 *Research* **2022** 9798679
[9] Zhou M G, Liu Z P, Yin H L, Li C L, Xu T K and Chen Z B 2023 *Research* **6** 0134
[10] Chen G, Chen Q, Long S, Zhu W, Yuan Z and Wu Y 2023 *Pattern Anal. Applic.* **26** 655
[11] Venegas-Andraca S E and Bose S 2003 *Proc. SPIE* **5105** 137
[12] Venegas-Andraca S E and Ball J 2010 *Quantum Inf. Process.* **9** 5
[13] Latorre J I 2005 arXiv:quant-ph/0510031
[14] Le P Q, Dong F and Hirota K 2011 *Quantum Inf. Process.* **10** 63
[15] Zhang Y, Lu K, Gao Y and Wang M 2013 *Quantum Inf. Process.* **12** 2833
[16] Zhang Y, Lu K, Gao Y and Xu K 2013 *Quantum Inf. Process.* **12** 3103
[17] Zhou R G, Yang P L, Liu X A and Ian H 2018 *Int. J. Quantum Inform.* **16** 1850060
[18] Jiang N and Wang L 2015 *Quantum Inf. Process.* **14** 1559
[19] Zhou R, Hu W, Luo G, Liu X and Fan P 2018 *Quantum Inf. Process.* **17** 7
[20] Zhou R G, Hu W, Fan P and Ian H 2017 *Sci. Rep.* **7** 2511
[21] Gao C, Zhou R G and Li X 2023 *Chin. Phys. B* **32** 050303

[22] Zhang Y, Lu K, Xu K, Gao Y and Wilson R 2015 *Quantum Inf. Process.* **14** 1573
[23] Zhang Y, Lu K and Gao Y 2015 *Sci. China Inf. Sci.* **58** 4
[24] Zhou R G, Tan C and Ian H 2017 *Int. J. Theor. Phys.* **56** 1382
[25] Le P Q, Iliyasu A M, Dong F and Hirota K 2011 *Theor. Comput. Sci.* **412** 1406
[26] Le P Q, Dong F and Hirota K 2010 *IAENG Int. J. Appl. Math.* **40** 3
[27] Luo G, Zhou R G, Liu X, Hu W and Luo J 2018 *Int. J. Theor. Phys.* **57** 2447
[28] Jiang N, Dang Y and Wang J 2016 *Quantum Inf. Process.* **15** 3543
[29] Dang Y, Jiang N, Hu H and Zhang W 2017 *Quantum Inf. Process.* **16** 4
[30] Li H S, Qingxin Z, Lan S, Shen C Y, Zhou R and Mo J 2013 *Quantum Inf. Process.* **12** 2269
[31] Caraiman S and Manta V I 2015 *Quantum Inf. Process.* **14** 1693
[32] Zhou R G, Hu W, Fan P and Luo G 2018 *Int. J. Quantum Inform.* **16** 1850021
[33] Zhou R G, Hu W and Fan P 2017 *Quantum Inf. Process.* **16** 9
[34] Yang Y G, Wang Y and Zhao Q Q 2016 *Multimedia Systems* **22** 271
[35] Yang Y G, Jia X, Xu P and Tian J 2013 *Quantum Inf. Process.* **12** 2765
[36] Heidari S and Naseri M 2016 *Int. J. Theor. Phys.* **55** 4205
[37] Zhou R G, Yang P L, Liu X A and Ian H 2018 *Int. J. Quantum Inform.* **16** 1850060
[38] Heidari S and Farzadnia E 2017 *Quantum Inf. Process.* **16** 242
[39] Jiang N and Wang L 2015 *Int. J. Theor. Phys.* **54** 1021
[40] Jiang N, Zhao N and Wang L 2016 *Int. J. Theor. Phys.* **55** 107
[41] Lomont C 2003 arXiv:quant-ph/0309070
[42] Yuan S, Mao X, Zhou J and Wang X 2017 *Int. J. Theor. Phys.* **56** 2495
[43] Yuan S, Lu Y, Mao X, Luo Y and Yuan J 2018 *Int. J. Theor. Phys.* **57** 804
[44] Sang J, Wang S and Li Q 2017 *Quantum Inf. Process.* **16** 42
[45] Wang J, Jiang N and Wang L 2015 *Quantum Inf. Process.* **14** 1589